Interaction network analysis in shear thickening suspensions

Marcio Gameiro, Abhinendra Singh, Lou Kondic, Konstantin Mischaikow, and Jeffrey F. Morris

Interaction network analysis in shear thickening suspensions

Marcio Gameiro,[1,2,*] Abhinendra Singh,[3,4,5,†] Lou Kondic,[6,‡] Konstantin Mischaikow,[2,§] and Jeffrey F. Morris[3,7,¶]

[1]*Instituto de Ciências Matemáticas e de Computação,*
Universidade de São Paulo,Caixa Postal 668, 13560-970, São Carlos, SP, Brazil
[2]*Department of Mathematics, Rutgers, The State University of New Jersey, Piscataway, NJ, 08854, USA*
[3]*Benjamin Levich Institute, CUNY City College of New York, New York, NY 10031, USA*
[4]*Pritzker School of Molecular Engineering, University of Chicago, Chicago, Illinois 60637, USA*
[5]*James Franck Institute, University of Chicago, Chicago, Illinois 60637, USA*
[6]*Department of Mathematical Sciences, New Jersey Institute of Technology, Newark, NJ 07102, USA*
[7]*Department of Chemical Engineering, CUNY City College of New York, New York, NY 10031*
(Dated: February 22, 2020)

Dense frictional particulate suspensions in a viscous liquid undergo increasingly strong continuous shear thickening (CST) as the solid packing fraction, ϕ, increases above a critical volume fraction, and discontinuous shear thickening (DST) is observed for even higher packing fractions. Recent studies have related shear thickening to a transition from mostly lubricated to predominantly frictional contacts with the increase in stress, with the transition determined by overcoming a repulsive force. The rheology and networks of frictional forces from two and three dimensional simulations of shear-thickening suspensions are studied. These are analyzed using measures of the topology of the network, including tools of persistent homology. We observe that at low stress the frictional interaction networks are predominantly quasi-linear along the compression axis. With an increase in stress, the force networks become more isotropic, forming loops in addition to chain-like structures. The topological measures of Betti numbers and total persistence provide a compact means of describing the mean properties of the frictional force networks, and provide a link between macroscopic rheology and the microscopic interactions. A total persistence measure describing the significance of loops in the force network structure, as a function of stress and packing fraction, shows behavior similar to that of relative viscosity, and displays a scaling law near the jamming fraction for both two and three dimensional systems considered. The total persistence measures for both dimensions are found to be very similar.

I. INTRODUCTION

In suspensions of solid particles in viscous liquid, an increase in viscosity with increasing shear rate or imposed stress is well-known, and is called shear thickening. If the particles are highly concentrated (or "dense"), such that the conditions approach the maximum flowable solid fraction (ϕ_A or ϕ in 2- or 3-dimensions, respectively), a very sharp increase in viscosity over a narrow range of shear rate may occur. This is termed "discontinuous shear thickening."

Recent simulation studies [1–5] have employed fluid mechanics based approach as a model leading to strong shear thickening. Within this approach, a breakdown of lubrication films between particles is responsible for the shear thickening behavior; phenomenological theories [6–8] containing the same basic elements are successful in predicting the flow behavior. It should be noted that alternative models not based on lubrication forces have been considered as well [9, 10].

The recent studies describing a stress-induced frictional rheology find a relationship between strong shear

thickening and shear jamming, in the sense that thickening may be a precursor to jamming: increase of either stress or solid fraction from a shear-thickening condition may lead to shear jamming. To be specific, shear jamming is the phenomenon of generating a solid structure under shear, but with this solid being fragile in the sense that it loses its ability to bear a shearing load (stress) without deformation if the load direction is changed sufficiently [11]. This loss of solidity is a temporary material failure, as rearrangement of structure, and in particular of the contact network, should once again result in jamming in the new direction of motion [12, 13]. Furthermore, one may wonder whether it is the contact network that is relevant to the process of shear-thickening and shear-induced jamming, or whether one needs to consider not only contacts, but also their strength. If strength of the contacts is considered as well, the concept of a weighted interaction network is introduced. Examples include weak or strong interaction networks considered commonly when analyzing dry granular matter, with so-called 'force chains' being the most commonly considered structures.

In shear-thickening suspensions, large changes in both the viscosity and the normal stress response have been associated with formation of a contact network driven by increasing shear stress. This prompts us to focus on the connectivity properties of this network, and its relation to stress transmission. Essential questions relate to how the connectivity arises, how it depends on the interaction

---

* gameiro@icmc.usp.br
† asingh.iitkgp@gmail.com
‡ Corresponding author: kondic@njit.edu
§ mischaik@math.rutgers.edu
¶ morris@ccny.cuny.edu

force strength, what are the geometrical and topological properties of the connected structures, and how these structures evolve with both the solid fraction and the imposed stress. All of these issues must be examined for a specific model of the microscopic physics.

We apply a discrete-particle simulation model that, using a minimal set of ingredients, has been found to closely approximate behavior observed in experiments [1–4]. This model assumes that particle surface separation is maintained by a repulsive force, and is thus lubricated by the liquid film that remains, until the applied stress overwhelms this repulsive force [1, 2]. In practice, many suspensions have steric or electrostatic forces, repulsive in either case, between particles to stabilize against surface contact, reducing aggregation or contact interactions. This leads to better flowability, i.e., lower viscosity and less of a tendency to jam. Such a repulsive force, of magnitude F_0, gives rise to a stress scale $\sigma_0 = F_0/6\pi a^2$ for particles of radius a, and within our simulational model or the theory of Wyart & Cates [7], this stress level marks the crossover from lubricated to contact frictional interactions between particle surfaces. At low stress, $\sigma \ll \sigma_0$, particle interactions are lubricated (and hence frictionless) and the viscosity is relatively low, diverging at random close packing (RCP) at a solid fraction that we denote by ϕ_J^0, with the subscript J indicating jamming. On the other hand, at high stress, $\sigma \gg \sigma_0$, most close interactions are frictional contacts, and the viscosity is both much larger and diverges at a solid fraction $\phi_J^\mu < \phi_J^0$; ϕ_J^0 depends on the interparticle friction [2]. With increase in stress, the transition between these two states results in shear thickening. Based on the value of packing fraction ϕ relative to the frictional jamming point ϕ_J^μ, different forms of shear–thickening can be observed. For $\phi \ll \phi_J^\mu$, the relation between shear rate $\dot{\gamma}$ and shear stress σ is monotonic, leading to continuous shear thickening (CST), while for larger ϕ the more abrupt discontinuous shear thickening (DST) may occur.

To gain better insight to the lubricated-to-frictional rheology transition, we apply tools of topology, with a focus on the network theoretical methodology of *persistent homology*, which has previously been applied to the closely related question of jamming in dry granular systems [14–16]. Alternate approaches [17–19] have been applied to elucidate the role of strong and weak networks in dry granular systems under shear. Persistent homology provides precisely defined and quantitative measures of the global interaction network, which is built on top of the contact network, as discussed in Section II B. In the present context, we use these tools to characterize flowing steady states, and thus the statistical properties of the interaction networks formed under different conditions in shear-thickening suspensions.

We point out two features of the analysis of interaction networks based on persistent homology that distinguish it from alternative approaches. First, this type of analysis naturally includes information about the forces between particles, and allows for quantification and comparison of the interaction networks, both between different states of a system, and between different systems. Second, this approach applies to both two- and three-dimensional (2D and 3D) phenomena. This is convenient, since the 2D case allows for development of intuition and visual demonstration of the tools applied here, while 3D results are in accord with physical experiment. The ability of the persistent homology tools to be applied without change of definition to 3D contact networks is an advantage for this method over complementary approaches to exploration of networks; see [20] for a review. We develop this approach here, demonstrating that measures of the structure determined by persistent homology show sharp changes where the rheology of the material undergoes abrupt shear thickening.

II. BACKGROUND & METHODS

A. Suspension flow simulation

We simulate simple shear flow of an assembly of non-Brownian frictional spheres (a monolayer in the two dimensional case) immersed in a Newtonian fluid under an imposed stress using Lees-Edwards periodic boundary conditions [21]. To avoid ordering, bidisperse particles with radii a and $1.4a$ are mixed at equal volume fractions. The particles interact through near-field forces of fluid mechanical origin (i.e., lubrication forces) and frictional contacts. This simulation scheme has been shown to reproduce many features seen experimentally in shear-thickening of dense suspensions [1, 2]. We consider the motion to be inertialess (at zero Reynolds number) so that the equation of motion reduces to force balance between lubrication ($\mathbf{F}_H$) and contact ($\mathbf{F}_C$) forces on each particle,

$$0 = \mathbf{F}_H(\mathbf{r}, \mathbf{u}) + \mathbf{F}_C(\mathbf{r}) , \qquad (1)$$

where $\mathbf{u}$ and $\mathbf{r}$ are written here as the many-body position and velocity vectors ($\mathbf{u} \equiv \dot{\mathbf{r}}$). A similar torque balance applies. To allow contact, the lubrication resistance singularity is cut off at a surface separation $h = 10^{-3}a$. The contact interactions are modeled using the approach of Cundall & Strack [22]. The tangential force between two particles is limited according to the Coulomb friction law to be no larger than the friction coefficient μ times the normal force, i.e. $\left|\mathbf{F}_C^t\right| \le \mu\left|\mathbf{F}_C^n\right|$, for compressive normal forces.

To incorporate rate dependence, we employ a Critical Load Model (CLM), in which an interparticle normal force threshold F_0 must be applied to activate friction between particles [1, 2, 5]. In this study we use an interparticle friction coefficient of $\mu = 1.0$. The apparent viscosity of the suspension is defined as $\eta = \sigma/\dot{\gamma}$, where $\dot{\gamma}$ is the shear rate of the simple shear flow, i.e., du_x/dy. The viscosity is presented through its form relative to the fluid viscosity $\eta_r = \eta/\eta_0$, where η_0 is the pure fluid value.
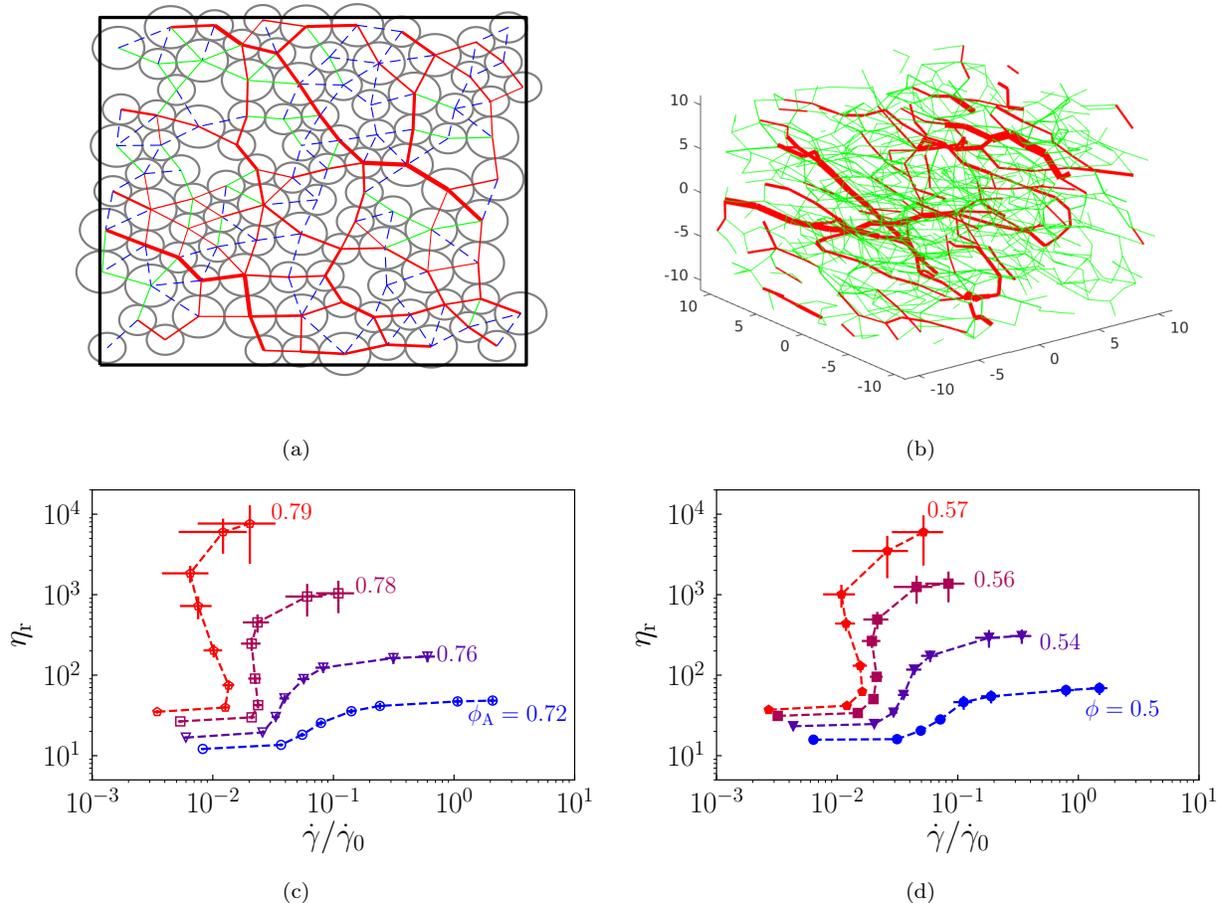
FIG. 1: (a-b) Snapshots of the force network at $\tilde{\sigma} = 1$ for (a) $\phi_A = 0.78$ in 2D and (b) $\phi = 0.56$ in 3D. Line thickness is proportional to the normalized force F with red, green and blue lines showing frictional, frictionless contact, and lubrication interactions, respectively. (c-d) Relative viscosity, η_r, as a function of dimensionless shear rate $\dot{\gamma}/\dot{\gamma}_0$ in stress-controlled simulations in (c) 2D and (d) 3D for several packing fractions.

A large increase in η_r with increasing shear rate is found, and this is the shear thickening of interest.

The force F_0 sets a stress scale, $\sigma_0 = F_0/6\pi a^2$, for the onset of shear thickening. In the remainder of this work, we report quantities in terms of $\tilde{\sigma} = \sigma/\sigma_0$ and the scaled strain rate $\dot{\gamma}/\dot{\gamma}_0$ with $\dot{\gamma}_0 \equiv F_0/6\pi\eta_0 a^2$. We normalize the force by the imposed shear stress $\sigma_0 a^2$. We use $N = 2000$ particles for 2D simulations and $N = 500$ particles for 3D simulations in a unit cell; to test size dependence, $N = 1000$ and 2000 were considered in 3D for a few cases.

From the simulations, we determine particle positions, normal and tangential contact forces, and non-contact lubrication forces. We perform simulation at a given condition for 20 strain units and record the data at strain steps of 0.01. Figures 1(a) and 1(b) show snapshots from simulation with $\tilde{\sigma} = 1$ for packing fractions $\phi_A = 0.78$ and $\phi = 0.56$ in 2D and 3D, respectively. In these images, we show the frictional (red solid line) and frictionless contacts (dashed green lines), and lubrication interactions

(blue dashed lines). The thickness of each frictional segment is proportional to the normalized force level F acting at the contact. As we will see, the development of the contact network with increasing stress is responsible for significant changes in the rheological response of the suspension.

If only the forces of fluid mechanical origin are relevant, the suspension would be expected to exhibit a rate- or stress-independent relative viscosity, with close interactions lubricated. Similarly, lubrication interactions together with frictional contacts, but without the repulsive force, result in a rate-independent rheology. The rheological rate-dependence thus arises due to the shear force overwhelming the repulsive forces, modeled here by the CLM approach [2], to cause a change in the dominant stress generation mechanism. In our simulations, we use a controlled shear stress protocol [3], in which the shear rate $\dot{\gamma}$ fluctuates. The relative viscosity is given by $\eta_r = \tilde{\sigma}/\langle\dot{\gamma}/\dot{\gamma}_0\rangle$, where angle brackets imply time average.

In order to present the results of topology-based anal-

ysis in a visually transparent manner, we consider 2D before turning to 3D simulations, for which comparisons of the rheology to experimental work have been made [2, 4]. Figures 1(c) and 1(d) show η_r as a function of shear rate for four packing fractions in 2D and 3D, respectively. For the lowest packing fractions, namely $\phi_A \leq 0.76$ in 2D and $\phi \leq 0.54$ in 3D, η_r increases continuously between two rate-independent values: this is CST. At packing fractions of $\phi_A = 0.78$ in 2D and $\phi = 0.56$ in 3D, the viscosity increases at almost constant shear rate over a brief interval, indicating that these are approximately the packing fractions for onset of DST. For higher packing fractions, $\phi_A = 0.79$ and $\phi = 0.57$, the viscosity function becomes sigmoidal under imposed stress, indicating that the suspension is fully in the DST state [8]. Note that if the simulations at the larger fractions are performed at fixed rate, $\eta_r(\dot{\gamma}/\dot{\gamma}_0)$ is observed to change discontinuously rather than following the S-shaped curve [3, 7, 8].
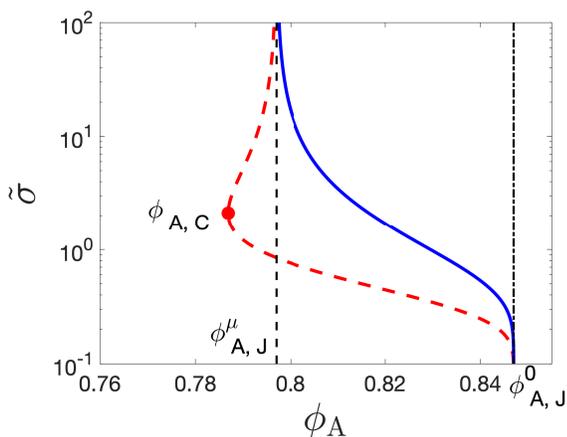

FIG. 2: Flow-state diagram in the shear stress versus 2D packing fraction $(\tilde{\sigma}, \phi_A)$ plane for $\mu = 1$; for the 3D version, see [8]. The red dashed line shows the locus of points for DST (where $\partial \dot{\gamma}/\partial \sigma = 0$) and the leftmost point on this curve is the minimum packing fraction, $\phi_{A,C}$, at which DST is observed. The blue solid curve shows packing fraction dependent maximum flowable stress above which the suspension is shear-jammed. Dashed and dotted-dashed black lines represent frictional ($\phi_{A,J}^\mu = 0.795$) and frictionless ($\phi_{A,J}^0 = 0.855$) jamming points in 2D, respectively.

Figure 2 shows a flow-state diagram, based on simulation results and a recently proposed model [8]; this particular diagram is for 2D, with the 3D version in the noted reference showing the same features. As discussed above, for the lower packing fractions $\phi_A < \phi_{A,C}$, CST is observed. For packing fractions $\phi_{A,C} \leq \phi_A < \phi_{A,J}^\mu$, DST is observed between two flowing states. For this range of ϕ_A, a curve shows the locus of DST points, i.e., $d\dot{\gamma}/d\sigma = 0$. For $\phi_A > \phi_{A,J}^\mu$, DST is observed between a flowing state (at low stress) and a shear jammed state and

is termed DST–SJ. The stress required to observe DST as well as shear jamming decreases with an increase in packing fraction. Both stresses vanish upon the approach to the frictionless jamming point. We do not consider the DST–SJ state further in this work, as the growth of the contact network with increasing stress is conceptually similar to the "pure" DST regime, while the subtleties of the network structure at jamming would expand beyond our desired scope. The goal here is to demonstrate the utility of topological data analysis as a tool for describing underlying features of the interaction networks resulting in the rheology of shear-thickening suspensions.

Recent studies have linked shear thickening with a growing number of frictional contacts as shear stress increases [1, 2, 5, 7]. Only limited work has explored the network properties of sheared suspensions [23, 24]. In the following, we focus on evolution of the network structure formed by the frictional forces. These are readily visualized in 2D, and Fig. 3 shows how the contact interaction network builds in 2D for stresses varying through the DST transition at $\phi_A = 0.79$. At low stress $\tilde{\sigma} = 0.1$, frictional contacts are absent, so that the suspension is in the low viscosity frictionless state. For $\tilde{\sigma} = 0.5$ and 1.0, the suspension begins to shear thicken, and frictional forces appear as roughly linear structures (force chains) along the compression axis, i.e. along $y = -x$ of the simple shear flow $u_x = \dot{\gamma}y$. With increase in stress to $\tilde{\sigma} \geq 2.0$, the suspension enters the DST regime and frictional interaction networks begin to form loops. With further increase in stress, the number of loops increases and saturates for $\tilde{\sigma} > 10$. Combined with the rheological curves in Fig. 1c, this illustrates the correlation between strong shear thickening and frictional interaction networks. Note that all structures described are transient, continuously forming, flowing, and breaking as the result of the bulk shearing motion.

B. Overview of topological measures: From Betti numbers to persistent homology

To introduce the relevant concepts, consider Fig. 4, which shows the interaction networks as a function of the interaction level, an *interaction network filtration* or simply a *filtration*; here the interparticle force is scaled by imposed stress $\sigma_0 a^2$. This figure illustrates the portions of the contact network experiencing force larger than the associated threshold or filtration level. At a very large force, only the most highly loaded contacts and the particles they connect are shown, and these are isolated objects. As the threshold is reduced, these components 'grow' and eventually merge with others. The information contained in such figures for a set of filtration levels will be used in what follows to formulate the relevant topological measures. Note that there is a visual similarity between the filtration at decreasing force threshold in Fig. 4 with the contact networks formed at increasing stress level in Fig. 3: although structural
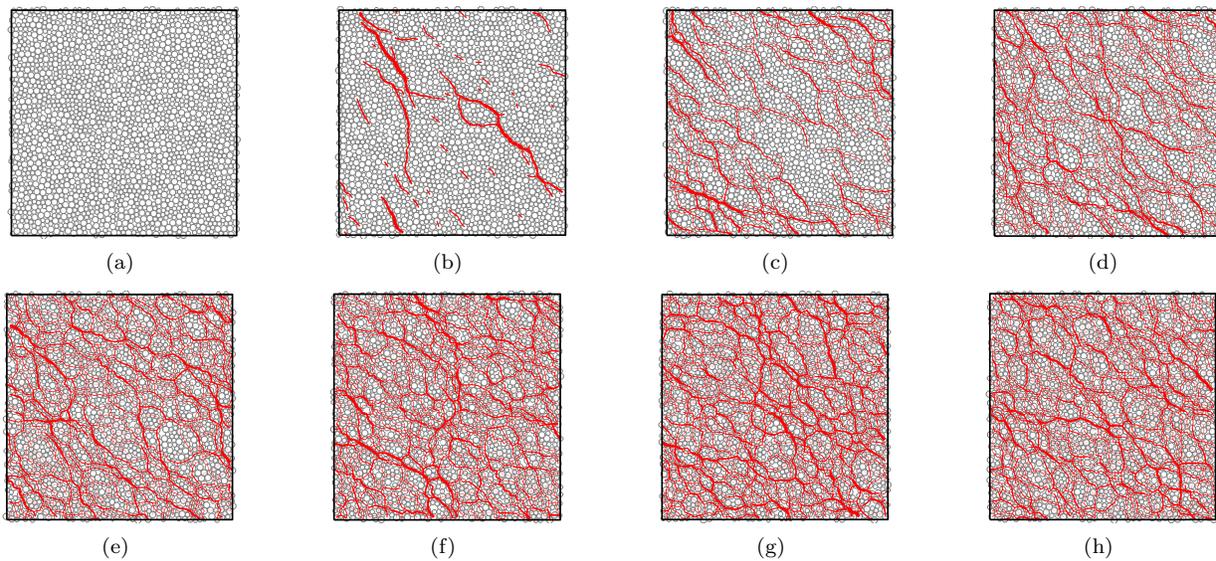
FIG. 3: Interaction network of all frictional contacts (normal force above the critical value, F_0) corresponding to a snapshot in steady state obtained in simulations with $\tilde{\sigma} =$ (a) 0.1, (b) 0.5, (c)1.0, (d) 2.0, (e) 5.0, (f) 10, (g) 50, and (h) 100 in 2D. Line thickness is proportional to the normalized force, F.
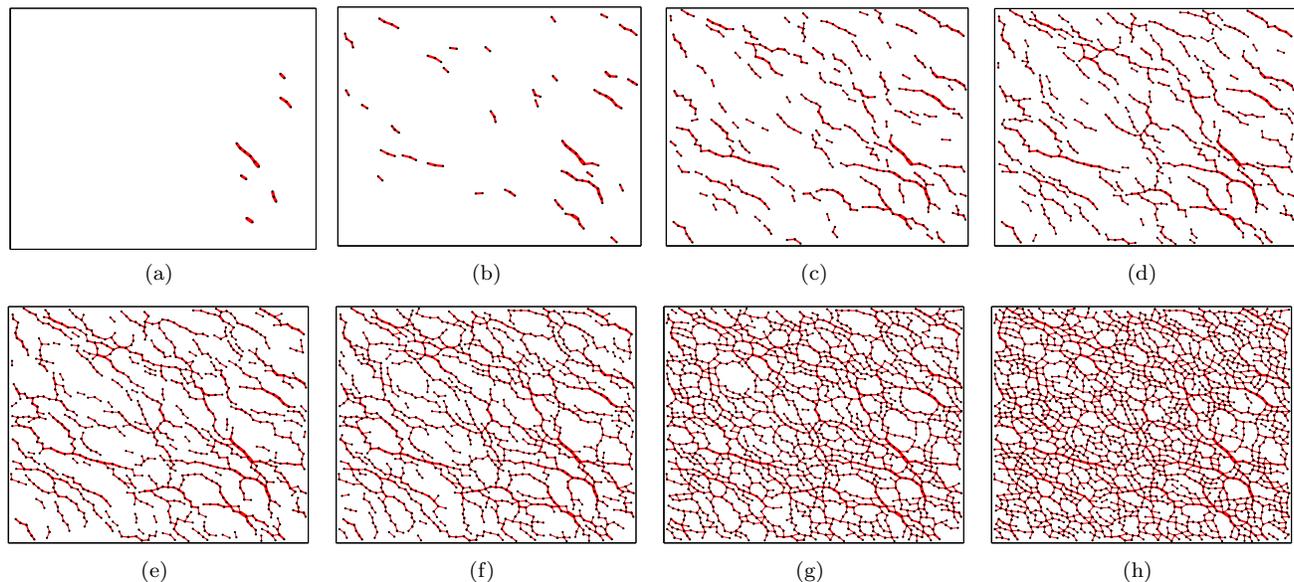

FIG. 4: Filtration of the interaction network of all frictional contacts for $\phi = \phi_A = 0.76$ and $\tilde{\sigma} = 10$ corresponding to a snapshot in steady state, for several values of the threshold, in order left to right and top to bottom: $F =$ (a) 4, (b) 3, (c) 2, (d) 1.6, (e) 1.3, (f) 1, (g) 0.5, and (h) 0. Here, black dots show particle centers and thickness of a red line corresponds to the strength of the normal force at the contact.

change takes place with increasing stress, the implication of this similarity is that the type of structures which are able to achieve the necessary force to generate a contact at low stress generate contacts which have the largest forces at elevated stresses where a fully ramified network forms.

To gain better insight into the structures that form, we consider Betti numbers, which specify the number of structures of a particulate type. The number of connected structures of any sort, from a contacting pair to an extended branched chain, is given by the zeroth Betti number, β_0, while the number of structures which form a closed loop is given by the first Betti number, β_1. The structures formed by connected particles enclosing a volume is given by the second Betti number, β_2, which is relevant in 3D, but not in 2D. We find no such structures in our 3D simulations (*i.e.*, $\beta_2 = 0$), and thus we only consider β_0 and β_1 in the following.

The manner of defining the structures is associated with a decreasing force threshold. As the force threshold

F decreases, 'birth' of a connected structure of a given Betti number is associated with the force threshold in a filtration for which the structure appears, i.e., it is the largest force within the structure. As the threshold is further decreased, the structure may grow in size as additional contacts are added. Consider a β_0 structure, formed at F_1, and a second that formed at $F_2 < F_1$; if these two structures merge, the resulting union results in the 'death' of one structure, and by definition it is the younger structure, which formed 'later' in the filtration (at lower force in a sequence of progressively reduced force threshold) which is lost, i.e., the structure with birth at F_2 dies upon the merging. The persistence of structures through the reduction of force threshold gives rise to the term persistent homology.
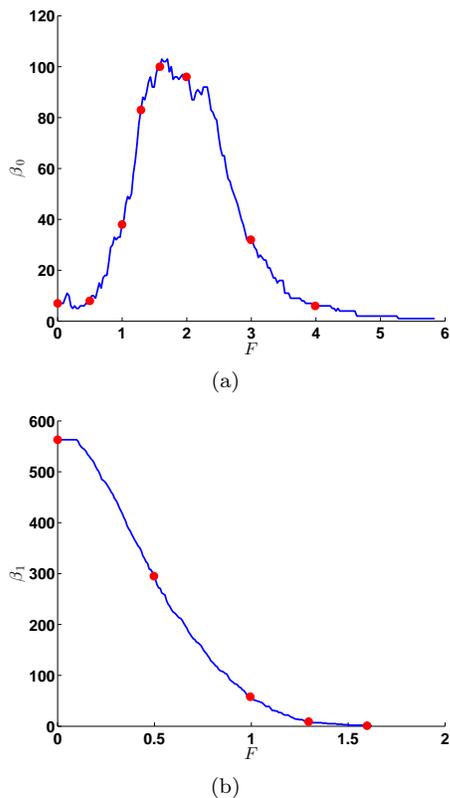

(a)

(b)

FIG. 5: Betti numbers corresponding to the filtration in Figure 4 for components (a) and loops (b). The (red) dots are at the force threshold levels corresponding to the values illustrated in Figure 4. Note the difference in the axes range for (a) and (b).

Figure 5 shows the Betti numbers for the configuration and network filtrations of Fig. 4; the red points in Fig. 5 correspond to the threshold levels shown in Fig. 4. We see from the β_0 plot that the maximum contact force level is slightly below $F = 6$. As the force threshold is decreased, β_0 increases monotonically until $F \approx 2.5$. Thus we see that connected structures are formed by contacts carrying different levels of force. The fact that there is a rapid increase in β_0 until $F \approx 2.2$ indicates that there

are many such components, with considerable variation in the force level.

Figure 5(b) shows that loops are absent until $F \approx 1.5$ and appear in significant numbers only for $F < 1$, which is well below the value at which the number of components starts decreasing rapidly. This implies that there is significant force heterogeneity, even on the level of single loops. To understand why, consider the formation of a loop at a given force level. Typically the loop forms as a single edge is added to a connected structure consisting of edges with higher forces. From Fig. 5(a) and 5(b) we infer that most loops form after many components of varying force intensity have merged. Thus, these loops are made up of components with a wide range of force levels. Furthermore, the fact that β_1 grows to much larger values than β_0 shows that the larger connected structures must contain numerous loops. This may be thought of as similar to the meshwork structure of a net, although it lacks the regularity of such a structure as shown by Fig. 4; a single connected piece of the mesh may contain from no loops to many loops, and the number and size of the loops is clearly mechanically relevant. Furthermore, the fact that the ratio β_1/β_0 decreases significantly as the force threshold is increased beyond $F = 1$ clearly illustrates a transition from structured network (with many loops) to more 'chainy' structure, as visualized also in Fig. 4. Further discussion of the insights that could be reached by considering Betti numbers for different threshold values and different stress values can be found in Sec. IV C.

While Betti numbers provide useful information regarding the number of components and loops, their utility is somewhat limited by the fact that they depend on the chosen force threshold, and therefore one needs to consider a large number of force threshold values to reach a reasonably complete understanding of the system. In addition, Betti numbers provide only the number of components and loops; they do not provide information about how these components and loops are connected. In principle, the system could even change its topological properties without a change of Betti numbers, e.g., a component could be born at essentially the same force level at which another component dies, and therefore the topology would change but β_0 would remain the same. Persistence diagrams allow us to deal with these concerns.

Figure 6 shows an example of such diagrams for β_0 and β_1. Here, for each structure, a point is placed at the (birth, death) coordinates (b, d). If a structure is still present at the minimum force threshold of the filtration, it is plotted (in red) with the coordinate pair $(b, -0.1)$ to illustrate that it was born at the threshold level b, and that it never dies. The (arbitrary) choice of -0.1 takes the corresponding points outside of the physically allowable values, in order to impart the information that these structures never die. In Fig. 6(a) the red point with $b \approx 6$ shows the component that formed first (at the largest threshold value), and this component by definition never
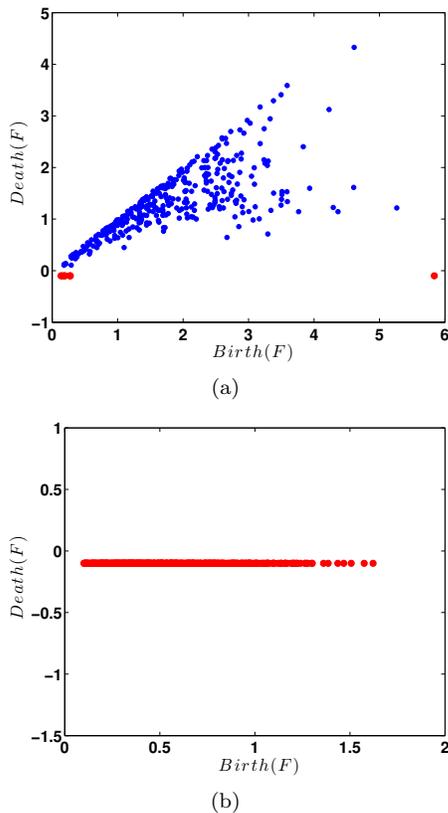
(a)

(b)

FIG. 6: Persistence diagrams corresponding to the filtration in Figure 4 for components (a) and loops (b).

dies. The red dots with $b \approx 0$ are specific to the system considered, and they show existence of separate components that form at very low threshold values. Such structures are possible due to fluid mechanical forces; in dry granular systems where only contact forces are present, such structures cannot form for a system in force balance, since they would imply unbalanced forces on the participating particles. We also note that our network filtrations (Fig. 4(b)) are formed by the particles and the edges representing the force interaction between them, and hence once a loop forms it never dies (loops cannot merge). The approach that we use here is slightly different from the one implemented elsewhere [14–16], where 'trivial' loops (formed by three adjacent particles) were not considered. In the present work, we find that including trivial loops influences the results only marginally, so we keep them in our calculations for simplicity.

Persistence diagrams provide a significant data reduction, expressing properties of complex weighted networks by a collection of points. However, these diagrams are essentially point clouds, and one needs to decide how to extract relevant information. While different approaches have been considered in earlier works [14–16, 25, 26], here we will focus on a single measure, the total persistence, which essentially quantifies how 'mountainous' is the interaction network, with larger distance from peaks

(where a structure is born) to a valley (where structures merge and one dies) contributing more to the total persistence measure. The total persistence τ_ℓ, $\ell = 0$ for components and $\ell = 1$ for loops, is defined as the sum of the distances of all points from the diagonal of a persistence diagram. More precisely,

$$\tau_\ell = \sum_{(b,d) \in PD_\ell} |d - b|$$

where we use the value $d = 0$ for the points in the persistence diagram PD_ℓ that never disappear, shown as $(b, -0.1)$ pairs in Fig. 6. In superficial terms, one could think of τ as a measure of the structure of the interaction network; larger total persistence means more structure. Conveniently, choosing τ as a measure reduces this complex structure to a pair of scalars. Clearly, considering total persistence instead of persistence diagrams leads to additional data reduction and loss of information. However, we will show that consideration of total persistence provides insight into the connection of topological properties of the interaction networks and rheology of the suspension. After discussing total persistence in what follows, we will return to persistence diagrams and Betti numbers to discuss how these relate to properties of interaction networks as the applied stress is varied, in both 2D and 3D.

III. TOTAL PERSISTENCE AS AN ORDER PARAMETER

Figure 7 shows the total persistence for 2D simulations at four packing fractions as a function of imposed stress. The data are obtained by averaging over 200 samples of the interaction network in the steady state at each $(\phi_A, \tilde{\sigma})$ condition; we show the mean and the standard deviation. The total persistence for the connected structures (τ_0) rises strongly in the transition region, from the low viscosity state at $\tilde{\sigma} < 1$ to the fully thickened one at $\tilde{\sigma} > 10$. The transition is even more distinct for the case of the loop (τ_1) structures, as the total persistence is essentially zero for $\tilde{\sigma} < 1$ and rises rapidly for $\tilde{\sigma} > 1$, again saturating at $\tilde{\sigma} \approx 10$; this saturated total persistence for β_1 is considerably larger for higher ϕ_A, with the value for $\phi_A = 0.79$ roughly double that at $\phi_A = 0.76$. The clear message is that the loop structures are more prevalent for the larger ϕ_A, and once formed many of these structures persist for all lower force thresholds: this is as expected on physical grounds, as the maximum force regions can be separated from one another, but stress continuity in the material requires that they be connected by lower force contacts.

The increase of the total persistence τ with both $\tilde{\sigma}$ and ϕ_A is directly correlated with the increase in the relative viscosity (and as shown elsewhere [2], there is a coincident increase in the normal stresses). The correlation between τ and η_r makes the total persistence useful as an order
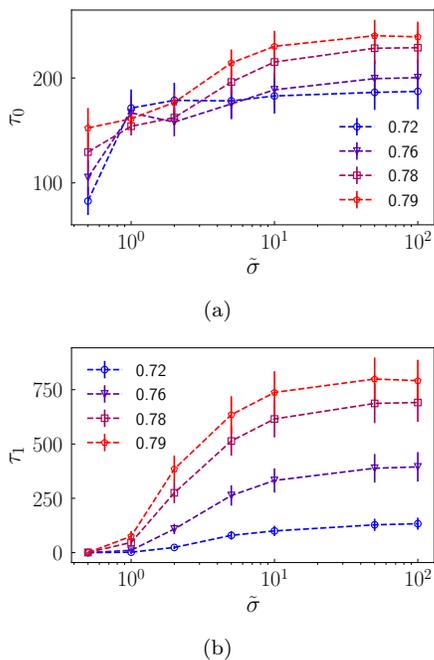
(a)

(b)

FIG. 7: Total persistence for 2D data as a function of $\tilde{\sigma}$ for components (a) and loops (b), for several values of packing fraction ϕ_A.

parameter that is indicative of a transition in the state of the material. This transition is manifested through the growth of total persistence as a function of imposed stress for an interaction network of frictional contacts, that form more abruptly and become stronger at larger ϕ_A.
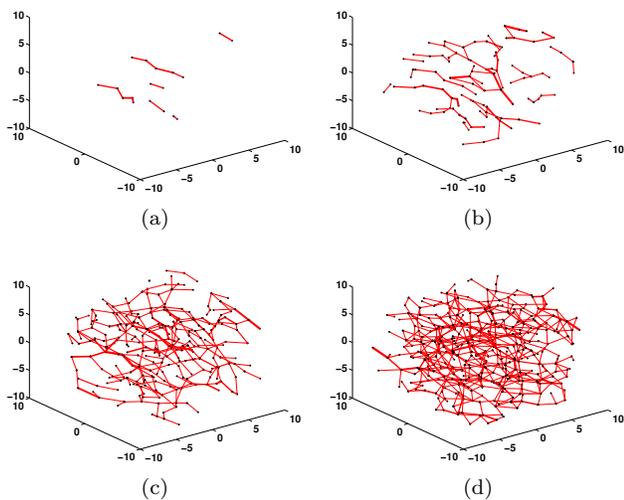

FIG. 8: Interaction networks for the 3D data for $\phi = 0.56$, for $\tilde{\sigma} = 0.5$ (a), $\tilde{\sigma} = 1$ (b), $\tilde{\sigma} = 2$ (c), and $\tilde{\sigma} = 10$ (d), each showing a single instant from the simulation once the structure has developed.

This observation is consistent with the picture emerging from the interaction networks displayed as a function of increasing stress in Fig. 3, or as a function of decreasing force threshold in the filtration illustrated by Fig. 4. While the 2D geometry allows ready visual identification of the network structure, the main interest is ultimately in 3D simulations. It is particularly valuable to have quantitative measures in 3D, where visualization is more difficult. The simulation approach used in this study has been shown to closely replicate experimental behavior [4]. The difficulty of identifying the networks in 3D flows is illustrated in Fig. 8 by snapshots of the contacting particles (shown as dots) and the forces (shown as connecting lines whose thicknesses indicate the magnitude of the force). The configurations are from simulations at $\phi = 0.56$ at varying imposed stress from $\tilde{\sigma} = 0.5$ to $\tilde{\sigma} = 10$, taken after sufficient strain, of $O(1)$, has been imposed to allow development of the structure. Unlike the equivalent network structures for 2D shown in Fig. 3, here we do not show the particles. Regardless of whether they are shown in a transparent form, the particles obscure the view, which even without the particles is clearly less enlightening than the equivalent 2D visualization.
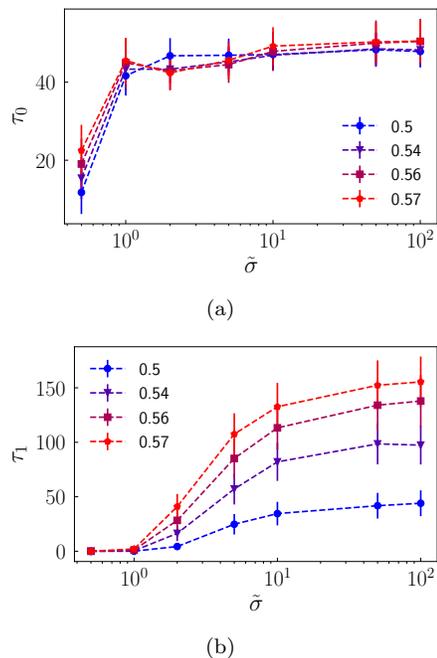

(a)

(b)

FIG. 9: Total persistence for 3D data as a function of $\tilde{\sigma}$ for components (a) and loops (b), for several values of packing fraction ϕ.

We thus turn to the persistent homology measures obtained from our 3D simulations, considering both the similarities with and differences from 2D. Figure 9 shows the total persistence for several ϕ. As stress increases, there is a rapid rise in τ_0 between $\tilde{\sigma} = 0.5$ and $\tilde{\sigma} = 1$, with near-saturation at $\tilde{\sigma} = 1$, while the loop structure measured by τ_1 begins to increase at $\tilde{\sigma} \approx 1$ and grows

up to $\tilde{\sigma} = 100$, with a slowing of the growth apparent above $\tilde{\sigma} = 10$. We thus find similarity in the measure of the interaction network structure, represented by the total persistence, and the viscosity transition seen in Fig. 1. In 3D, the variation of τ up to $\tilde{\sigma} = 100$ indicates that the interaction network structure continues to develop with increasing $\tilde{\sigma}$ well above the initial transition to the higher viscosity region.

To this point, all results we have presented for 3D were obtained from simulations with $N = 500$. One obvious question is how the results (for the total persistence in particular) vary with N. To answer this question, we have carried out additional 3D simulations with different numbers of particles. Figure 10 displays τ_0 and τ_1 for 3D simulations at $\phi = 0.56$ scaled by the value of N used for that case. We observe the data to collapse within the error bars; however, there does seem to be a weak trend of τ_0 decreasing as N increases, and the opposite trend for τ_1. This trend is explained by the boundary effects. The simulations are periodic in all directions, but this periodicity is not considered when computing the persistence diagrams. For this reason we miss the "across boundary" particle interactions. This has the effect of considering some components that are supposed to be connected "across the boundary" as two separated components, and hence it produces additional components (points in the diagrams in dimension 0). Additionally, some loops that are formed by connections "across the boundary" are not counted as loops, and hence we miss some loops (points in the diagrams in dimension 1). This effect is more noticeable for smaller systems, where the ratio of boundary area to volume increases.
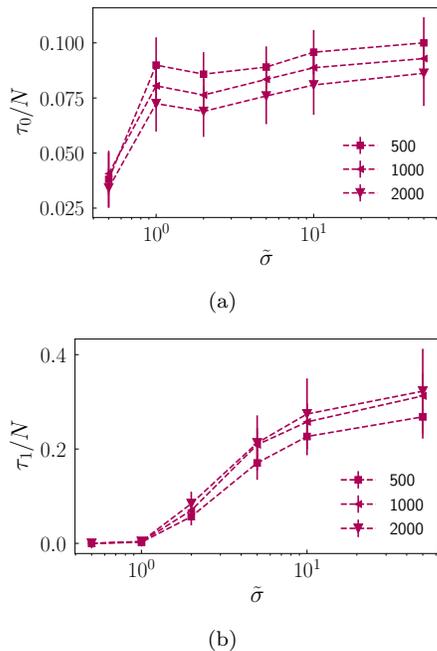
Figure 11 displays correlation in both 2D and 3D simulations between relative viscosity and total scaled persistence corresponding to loops, τ_1/N. This figure shows that the viscosity increases with τ_1/N, and appears to diverge at some maximum persistence. The dashed line shows $\eta_r \propto [(\tau_1^J - \tau_1)/N]^{-\alpha}$ where $\tau_1^J/N = \tau_1(\phi = 0.57, \tilde{\sigma} = 100)/N = 0.34$ (for 3D) and $\tau_1(\phi_A = 0.79, \tilde{\sigma} = 100)/N = 0.42$ (for 2D) and $\alpha = -1.8$. The higher–ϕ data, in which DST is seen, follow a single scaling law, while for packing fraction $\phi = 0.5$ and $\phi_A = 0.72$, the data does not agree with the proposed correlation. The structural implication is that the thickened state of DST is associated with a topology of the frictional interaction network similar to that in the jammed state. The observed correlation suggests that the viscosity is solely given by the microstructure, described by the total persistence. The persistence intrinsically is governed by the volume fraction (or distance from jamming point) and the applied stress. It is important to highlight that a given combination of $(\phi, \tilde{\sigma})$ that has the same τ_1 at the mesoscale, results in the same macroscopic behavior, i.e., relative viscosity.
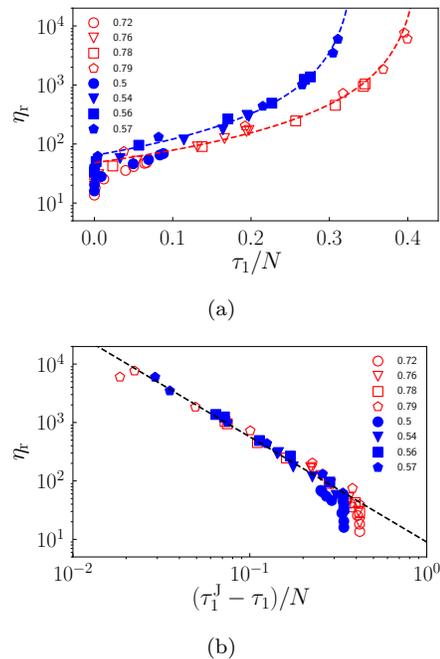

(a)

(b)

FIG. 11: (a) Relative viscosity η_r vs. scaled total persistence (dimension 1) τ_1/N for different packing fractions for 2 and 3 dimensional data. Solid and empty symbols are used for 2D and 3D, respectively. The dashed lines represent $\eta_r \propto [(\tau_1^J - \tau_1)/N]^{-\alpha}$ with $\tau_1^J/N = 0.34$ and 0.42 for 2D and 3D, respectively, and $\alpha = -1.8$. Red and blue symbols represent two and three dimensional data. (b) The same data on a log-log scale showing η_r vs $(\tau_1^J - \tau_1)/N$. The dashed line shows the power law of -1.8.

(a)

(b)

FIG. 10: Scaled total persistence for 3D data for $\phi = 0.56$ as a function of $\tilde{\sigma}$: (a) τ_0 and (b) τ_1.

IV. STRUCTURE OF INTERACTION NETWORKS

Here we consider insight to the structure of the interaction networks that can be gained from consideration of persistence diagrams and Betti numbers.

A. Interaction structure variation with stress

We address the question of how the structure of the interaction network changes as stress increases at fixed ϕ (or ϕ_A), and to answer this we turn to the persistence diagrams. Total persistence, τ, compresses all available information into a pair of numbers, and thus we seek insight from the additional information in the persistence diagrams from which these numbers are determined. Figure 12 shows the superposition of all β_0 persistence diagrams at each of seven values of imposed stress for the 2D simulations at $\phi_A = 0.79$. We observe that as $\tilde{\sigma}$ increases, the density of the points on the persistence diagrams increases. This is consistent with Fig. 7(a), and we see that once the thickened state is reached at $\tilde{\sigma} \approx 5$, the density of the points shows little further variation. We also note that for $\sigma > 1$, there is an increased number of points at lower right side of the diagrams, suggesting that the corresponding networks include more disconnected parts that live longer. In more general terms, we deduce that as the suspension reaches the thickened state, its primary structural properties are essentially unchanging, and thus the interaction forces on the contacts simply increase proportionally with the applied stress. This conclusion is supported by considering β_1 persistence diagrams (figure not shown for brevity).

B. Interaction structure variation with solid fraction

Here we consider whether the structure changes as one progresses from CST to DST at fixed stress, by modifying the packing fraction. Note that if there are significant changes in the structure of the interaction network, then we expect differences in the corresponding persistence diagrams. Examination of plots such as those shown in Fig. 12 at different packing fraction show only minor differences, consistent with total persistence results. Essentially, the only influence of packing fraction is a slight shift of the points in persistence diagrams to lower values for smaller packing fractions. Therefore, if the system is already in the thickened state, we do not find qualitative differences in the structure of interaction networks for the systems that are brought to thickened state by increasing either applied stress or packing fraction.

C. Role of physical dimensionality

We address finally whether and how the structure of interaction networks depends on the number of physical dimensions. We note that resolving the influence of dimensionality by considering purely topological measures is difficult, since the significant data reduction involved in computing homology may also remove relevant information about the structure. Nevertheless, to gain some basic insight, we default first to Betti numbers. Figure 13 shows the Betti numbers for the 2D and 3D simulations, scaled by the number of particles. We find that the Betti number curves are similar for 2D and 3D, especially for β_0 which is strikingly similar for the 2D and 3D at large stress, where the network structure has saturated; note that the value of peak shifts to larger F for 2D. The finding that Betti numbers are so similar for 2D and 3D is surprising, given the difference in number of near neighbors in 2D (about six) and 3D (about 12). If we now consider the relationship of total persistence to relative viscosity shown in Fig. 11, we find a similar scaling law for either 2D or 3D on approach to jamming. This is again surprising and intriguing, as the total persistence provides a compact description of the connectivity of the network, and this would *a priori* be expected to differ depending on dimensionality. Such expectations arise from noting that a mechanically stable static or jammed packing depends systematically on dimensionality D, varying from $Z = 2D$ to $D + 1$ as the friction coefficient varies from $\mu = 0$ to $\mu \to \infty$ [27]. Thus, we have identified similarities across dimensionality in both the Betti numbers for the high-stress, or 'fully-networked' conditions, and for the near-jamming total persistence of sheared suspension contact networks. This similarity between measures of 2D and 3D networks points to a need for a more thorough understanding of the relation of the network structure to the mechanical properties, as it may reveal principles of force organization in amorphous materials.

As a final note regarding Fig. 13, the flat portion of the β_0 and β_1 curves at smaller values of F and small $\tilde{\sigma}$ are due to lubrication forces that allow for existence of a non-zero number of components. For large values of $\tilde{\sigma}$ these separate components are not present since the applied stress is strong enough to make all components connect. A similar argument explains constant values of β_1 for the same values of force threshold.

V. CONCLUSION AND PERSPECTIVE

In this paper we have shown that there is a clear connection between the local properties of the interaction networks that develop in sheared suspensions and their global rheological response. This finding suggests that proper understanding of the properties of the interaction networks may be the key in quantifying their rheological response not only for relatively simple flow geometry considered here, but in other more complex settings as well.
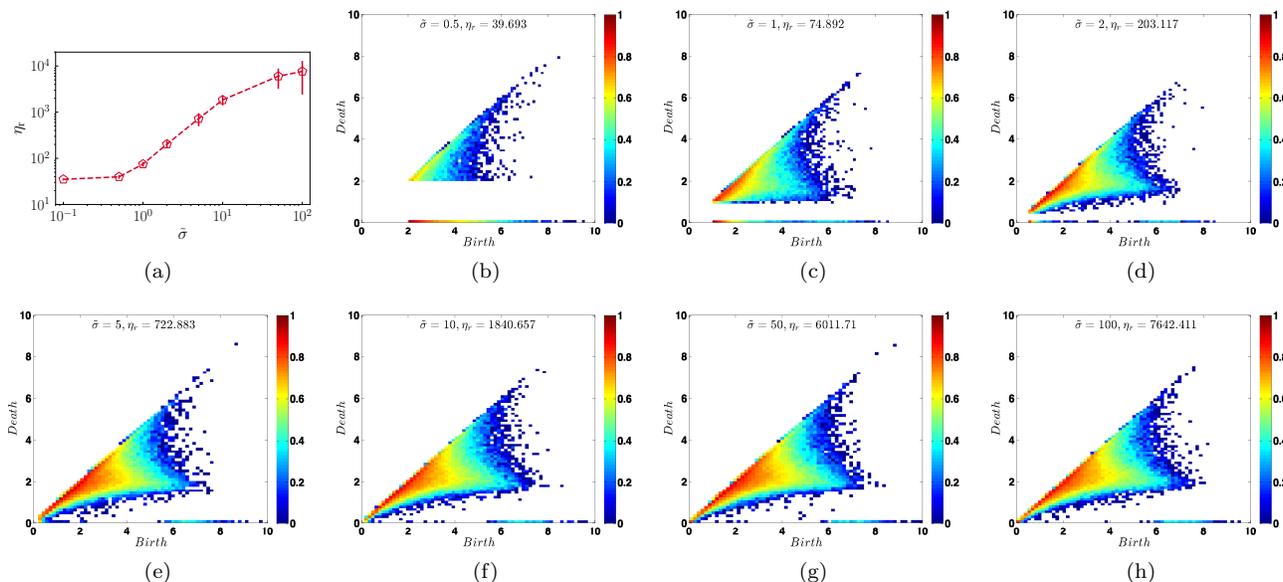
FIG. 12: (a) Relative viscosity η_r plotted as a function of stress $\tilde{\sigma}$ for area fraction $\phi_A = 0.79$. Density plots of all the β_0 persistence diagrams superimposed for the given parameters values for the 2D simulations colored according to the density of points. The color bar indicates the density normalized across all the plots. The plots correspond to $\phi_A = 0.79$ and for (b): $\tilde{\sigma} = 0.5$, (c): $\tilde{\sigma} = 1$, (d): $\tilde{\sigma} = 2$, (e): $\tilde{\sigma} = 5$, (f): $\tilde{\sigma} = 10$, (g): $\tilde{\sigma} = 50$, (h): $\tilde{\sigma} = 100$.

It is encouraging that a relatively simple measure, the total persistence describing structure of loops in the interaction networks, appears as an order parameter that describes well the rheology. This finding is important, since it suggests that the details of the interaction networks may be absorbed into a compact measure for the purpose of understanding the rheology. On the other hand, it should be noted that the total persistence includes (in compressed form) the information about interaction network properties for all interaction strengths at once, and therefore understanding and quantifying particle-particle interactions may be needed for the purpose of describing the material response.

One particularly interesting finding is that the total persistence *of loops in interaction networks* is the measure that correlates the best with the rheological properties (viscosity). This result suggests that future research should focus in more detail on the connectivity of the interaction networks in order to understand better the rheology. It remains to be seen whether the fact that the total persistence of loops in particular appears as an order parameter describing the system behavior remains valid for more complex systems.

Our results show that the considered topological measures, both the simple ones (Betti numbers) and more complex ones (total persistence) appear very similar for the two and three dimensional suspension flows studied. Since the number of contacts and the geometry of particle packing are strongly dependent on the number of physical dimensions, one wonders whether there is some additional not yet discovered property of the interaction networks that leads to their dimension-independent prop-

erties.

The interaction networks clearly play an important role in quantifying rheological response of sheared suspensions. While these networks are complex, particularly when considered for all interaction strengths at once, persistent homology provides a way towards their analysis and quantification, removing a significant amount of complexity and isolating rather straightforward measures that could be used to quantify the rheology. Our results suggest that a similar type of analysis may be of utility for the purpose of describing many other systems such that the interaction between the basic building blocks can be described in terms of interaction networks. We also note the potential for using persistent homology to analyze temporal evolution of evolving networks. Established measures for computing correlations between networks at different times exist, and we expect that significant new insight could be gained by applying such measures and comparing them with evolving rheological properties.
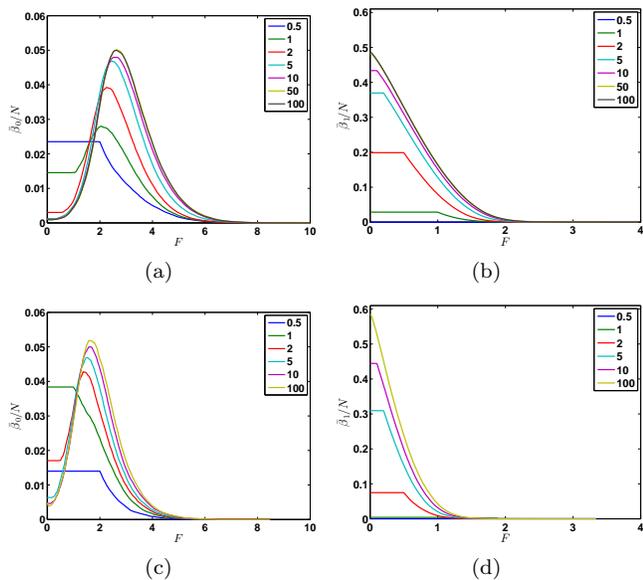
FIG. 13: Betti numbers for several values of $\tilde{\sigma}$, scaled by the number of particles N for 2D simulations (a-b) for $\phi_A = 0.79$, and for 3D simulations (c-d) for $\phi = 0.56$. Parts (a, c) show β_0, and (b, d) show β_1. Here we have analyzed only the frictional contacts, i.e, contacts for which force is larger than the critical normal force F_0 and is normalized with the applied stress. Since there are no frictional contacts for $F < F_0$, Betti number plateaus for small forces and due to the normalization with applied stress the onset of plateau decreases with increase in stress.

[1] R. Seto, R. Mari, J. F Morris, and M. M Denn. Discontinuous shear thickening of frictional hard-sphere suspensions. *Phys. Rev. Lett.*, 111(21):218301, 2013.

[2] R. Mari, R. Seto, J. F Morris, and M. M. Denn. Shear thickening, frictionless and frictional rheologies in non-brownian suspensions. *J. Rheol.*, 58(6):1693–1724, 2014.

[3] R. Mari, R. Seto, J. F Morris, and M. M. Denn. Non-monotonic flow curves of shear thickening suspensions. *Phys. Rev. E*, 91(5):052302, 2015.

[4] R. Mari, R. Seto, J. F. Morris, and M. M. Denn. Discontinuous shear thickening in brownian suspensions by dynamic simulation. *Proc. Natl. Acad. Sci.*, 112(50):15326–15330, 2015.

[5] C. Ness and J. Sun. Shear thickening regimes of dense non-brownian suspensions. *Soft Matt.*, 12(3):914–924, 2016.

[6] I. A. Bashkirtseva, A. Yu. Zubarev, L. Yu. Iskakova, and L. B. Ryashko. On rheophysics of high-concentrated suspensions. *Colloid Journal*, 71(4):446–454, 2009.

[7] M. Wyart and ME Cates. Discontinuous shear thickening without inertia in dense non-brownian suspensions. *Phys. Rev. Lett.*, 112(9):098302, 2014.

[8] A. Singh, R. Mari, M. M. Denn, and J. F. Morris. A constitutive model for simple shear of dense frictional suspensions. *J. Rheol.*, 62(2):457–468, 2018.

[9] C. Heussinger. Shear thickening in granular suspensions: inter-particle friction and dynamically correlated clusters. *Phys. Rev. E*, 88:050201(R), 2013.

[10] J. Dong and M. Trulsson. Analog of discontinuous shear thickening flows under confining pressure. *Phys. Rev. Fluids*, 2(8):081301, 2017.

[11] M. E. Cates, J. P. Wittmer, J.-P. Bouchaud, and P. Claudin. Jamming, force chains and fragile matter. *Phys. Rev. Lett.*, 81:1841, 1998.

[12] R. Seto, A. Singh, B. Chakraborty, M. M. Denn, and J. F. Morris. Shear jamming and fragility in dense suspensions. *Gran. Matt.*, 21(3):82, Aug 2019.

[13] A. Singh, S. Pednekar, J. Chun, M. M Denn, and J. F Morris. From yielding to shear jamming in a cohesive frictional suspension. *Phys. Rev. Lett.*, 122(9):098004, 2019.

[14] M. Kramár, A. Goullet, L. Kondic, and K. Mischaikow. Quantifying force networks in particulate systems. *Physica D*, 283:37, 2014.

[15] M. Kramár, A. Goullet, L. Kondic, and K. Mischaikow. Persistence of force networks in compressed granular media. *Phys. Rev. E*, 87:042207, 2013.

[16] M. Kramár, A. Goullet, L. Kondic, and K. Mischaikow. Evolution of force networks in dense particulate media. *Phys. Rev. E*, 90:052203, 2014.

[17] E. Azéma and F. Radjai. Internal structure of inertial granular flows. *Phys. Rev. Lett.*, 112(7):078001, 2014.

[18] D. Cantor, E. Azéma, P. Sornay, and F. Radjai. Rheology and structure of polydisperse three-dimensional packings of spheres. *Phys. Rev. E*, 98(5):052910, 2018.

[19] E. Azéma and F. Radjai. Force chains and contact network topology in sheared packings of elongated particles. *Phys. Rev. E*, 85(3):031303, 2012.

[20] L. Papadopoulos, M. Porter, K. Daniels, and D. Bassett. Network analysis of particles and grains. *J. Complex Networks*, 6:485, 2018.

[21] A. W. Lees and S. F. Edwards. The computer study of transport processes under extreme conditions. *J. Phys. C.*, 5(15):1921, 1972.

[22] P. A. Cundall and O. D. L. Strack. A discrete numerical model for granular assemblies. *Geotechnique*, 29:47–65, 1979.

[23] L. E. Edens, S. Pednekar, J. F. Morris, G. K. Schenter, A. E. Clark, and J. Chun. Global topology of contact force networks: Insight into shear thickening suspensions. *Phys. Rev. E*, 99(1):012607, 2019.

[24] J. E. Thomas, K. Ramola, A. Singh, R. Mari, J. F Morris, and B. Chakraborty. Microscopic origin of frictional rheology in dense suspensions: correlations in force space. *Physical Rev. Lett.*, 121(12):128002, 2018.

[25] L. A. Pugnaloni, C. M. Carlevaro, M. Kramár, K. Mischaikow, and L. Kondic. Structure of force networks in tapped particulate systems of disks and pentagons I: Clusters and Loops. *Phys. Rev. E*, 93:062902, 2016.

[26] L. Kondic, M. Kramár, L. A. Pugnaloni, C. M. Carlevaro, and K. Mischaikow. Structure of force networks in tapped particulate systems of disks and pentagons II: Persistence analysis. *Phys. Rev. E*, 93:062903, 2016.

[27] A. J. Liu and S. R. Nagel. The jamming transition and the marginally jammed solid. *Annu. Rev. Condens. Matter Phys.*, 1(1):347–369, 2010.